

## Human Brain: Proton Diffusion MR Spectroscopy<sup>1</sup>

Diffusion of brain metabolites was measured in 10 healthy volunteers by using localized proton diffusion magnetic resonance (MR) spectroscopy. Measurements were conducted with a clinical MR imager by using a stimulated-echo pulse sequence (3,000/60 [repetition time msec/echo time msec], 200-msec mixing time) with additional outside-volume suppression. Motion artifacts due to macroscopic brain movements were compensated by means of peripheral cardiac gating and separate collection of individual spectroscopic acquisitions into a two-dimensional data matrix. Phase errors due to macroscopic motion were subsequently corrected in individual data traces prior to spectral averaging. Mean ( $\pm 1$  standard deviation) apparent diffusion coefficients of choline-containing compounds ( $[0.13 \pm 0.03] \times 10^{-3}$  mm<sup>2</sup>/sec), creatine and phosphocreatine ( $[0.15 \pm 0.03] \times 10^{-3}$  mm<sup>2</sup>/sec), and *N*-acetyl aspartate ( $[0.18 \pm 0.02] \times 10^{-3}$  mm<sup>2</sup>/sec) were substantially smaller than that of water and were consistent with recently published data obtained in anesthetized and paralyzed animals. Adequate diffusion sensitivity for metabolites in the human brain can be obtained with clinical whole-body imagers despite macroscopic head and brain movements.

**Index terms:** Brain, perfusion, 13.12144, 13.12145, 15.12144, 15.12145 • Magnetic resonance (MR), diffusion study, 13.12144, 15.12144 • Magnetic resonance (MR), spectroscopy, 13.12145, 15.12145 • Magnetic resonance (MR), tissue characterization

**Radiology 1993; 188:719-725**

**M**AGNETIC resonance (MR) imaging of water self-diffusion may provide useful information about tissue structure and function, as diffusion coefficients in vivo are related to cellular parameters such as dimensionality, compartmentation, and transport processes (1-3). For instance, diffusion MR imaging provides valuable information about white matter fiber orientation in the central nervous system (4,5) on the basis of anisotropic diffusion. Diffusion MR imaging also appears promising in the evaluation and management of brain infarctions at a very early stage when findings of other modalities, including T1- and T2-weighted MR imaging, are still normal (6,7).

To date, however, diffusion measurements in humans have been performed only on water, for reasons of technical feasibility. Water may not be the most suitable molecule for diffusion measurements because of its ubiquity and the permeability of most tissue interfaces, such as membranes, to water molecules. In this context, diffusion measurements of more complex molecules that are tissue-specific appear to be promising for tissue characterization.

Such measurements are technically more challenging, because such molecules have a lower concentration than that of water. Recently, initial diffusion measurements of selected metabolites in vivo have been reported in brain and muscle tissue of anesthetized and paralyzed animals by using both localized phosphorus-31 and hydrogen-1 spectroscopy (8-10). The magnitudes and directional anisotropy of diffusion coefficients of molecules

such as choline-containing compounds (Cho), creatine and phosphocreatine (Cr-PCr), and *N*-acetyl aspartate (NAA) were found to be consistent with cell dimensions and orientations (8,9).

Applications of diffusion spectroscopy in humans have been less successful, probably because of the lack of adequate motion-compensation methods. Macroscopic motion due to involuntary subject movements, respiration, and cerebrospinal fluid-related brain pulsations may lead to an overestimation of diffusion coefficients in humans (11). Gradient compensation schemes to reduce artifacts from linear movements have been proposed (12,13). They require, however, substantially longer diffusion times to compensate for the loss in diffusion sensitivity (13). This requirement may be disadvantageous if diffusional restriction, which requires shorter diffusion times, is to be investigated. In addition, signal losses due to relaxation during the pulse sequence are increased. Shorter diffusion times are achievable with small-bore imagers, in which much stronger gradient strengths are available.

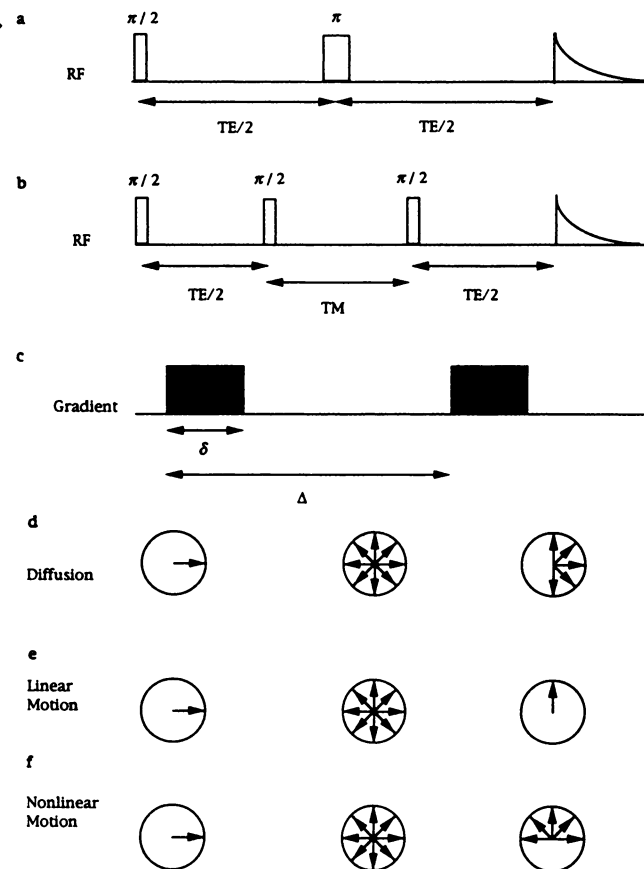
The purpose of this study was to demonstrate the feasibility of spectroscopic diffusion measurements of Cho, Cr-PCr, and NAA in human brain tissue with a clinical whole-body imager. A stimulated-echo pulse sequence with complete outer-volume presaturation (14) to improve volume localization is designed to increase diffusion sensitivity while limiting motion artifacts from head movements and cardiac-related brain pulsations. Signal losses due to mac-

<sup>1</sup> From the Department of Diagnostic Radiology, Warren Grant Magnuson Clinical Center (S.P., D.L.B.), and Laboratory of Diagnostic Radiology Research (C.A.C.), National Institutes of Health, Bldg 10, Rm 1C660, Bethesda, MD 20892. From the 1992 RSNA scientific assembly. Received January 14, 1993; revision requested March 4; revision received April 12; accepted April 16. S.P. supported by the Swiss National Science Foundation. Address reprint requests to S.P.

© RSNA, 1993

**Abbreviations:** CHES = chemical shift-selective, Cho = choline-containing compounds, Cr-PCr = creatine and phosphocreatine, NAA = *N*-acetyl aspartate, STEAM = stimulated-echo acquisition mode, TE = echo time, TM = mixing time.

**Figure 1.** Pulse sequences for diffusion measurements and effects of motion on the echo signal. *a*, Spin-echo sequence. *b*, Stimulated-echo sequence. *c*, Diffusion gradients are applied symmetrically in the  $TE/2$  (half echo time) periods.  $\delta$  is the duration of the diffusion gradients.  $\Delta$  is the time between the two diffusion gradients. The arrows in *d-f* depict the spin magnetization in the transverse plane after excitation (left), after the first diffusion gradient (center), and at the top of the echo (right). *d*, With pure diffusion the signal is dephased, but the net phase is unchanged. *e*, In the case of purely linear motion along the direction of the diffusion gradients, the signal amplitude is unchanged but the signal phase changes. *f*, With other forms of motion, both signal amplitude and phase changes occur.



roscopic motion are reduced by means of cardiac gating and compensating motion-induced phase errors in individual acquisitions. Results obtained in 10 healthy volunteers demonstrate that adequate diffusion sensitivity and motion artifact compensation can be achieved in conscious human subjects.

## MATERIALS AND METHODS

### Theory

Conventional spin-echo and stimulated-echo MR imaging can be sensitized to diffusion by symmetrically applying gradient pulses that attenuate the echo signal  $S$  (Fig 1). Assuming isotropic and unrestricted diffusion, the diffusion coefficient,  $D$ , can be determined by measuring the signal attenuation as a function of the gradient factor  $b$ , which is dependent on the radio frequency and gradient pulse sequence and increases with increasing gradient strength and pulse sequence timing (3,15):

$$S = S_0 \cdot \exp^{-Db}, \quad (1)$$

where  $S_0$  is the signal intensity without diffusion. In case of restricted diffusion (eg, due to cellular compartmentation) the measured diffusion coefficient becomes dependent on the pulse sequence timing. The diffusion coefficient is related to the root mean square displacement ( $\sqrt{\langle [x - x_0]^2 \rangle}$ ) in a given spatial direction by  $\sqrt{\langle [x - x_0]^2 \rangle} = \sqrt{2Dt_{diff}}$ , where  $t_{diff}$  is the diffusion time. For the pulse sequences in Figure 1,  $t_{diff}$  is defined as  $(\Delta - \delta/3)$ . For unrestricted diffusion  $\langle [x - x_0]^2 \rangle$  increases linearly with  $t_{diff}$ . In the case of motion restriction the relationship is nonlinear, with a leveling off where  $\langle [x - x_0]^2 \rangle$  reaches the size of the restricting compartment while the measured diffusion coefficient  $D$  decreases. The average signal phase shift due to pure diffusion is zero, since there is no net displacement of the spins under observation (Fig 1d).

By contrast, if net displacements of spins in the presence of field gradients are superimposed on diffusion, further signal phase changes and amplitude losses may occur in addition to amplitude losses due to diffusion (Fig 1, *e, f*). The additional effect of linear bulk motion (ie, along a given spatial direction) on the signal phase and amplitude can be determined by integrating the spin signals at the time

of the echo formation (echo time [TE]) neglecting relaxation and field inhomogeneity effects:  $S = \iiint \rho(r') \exp^{i\phi(r')} dr'$ , where  $\rho(r')$  is the local spin density and  $\phi(r') = \gamma \int_0^{TE} G(t') r''(t') dt'$ .

The  $\gamma$  represents the gyromagnetic ratio.  $G(t')$  is the effective gradient sequence in the direction of the movement as a function of time. Gradients prior to the refocusing pulse or pulses give negative contributions.  $r''(t')$  is the trajectory of the spin during the pulse sequence. For stationary nondiffusing spins the pulse sequence is symmetric and the spins are completely refocused at the center of the echo. For linear bulk motion (coherent translations along a given spatial direction) the phase dispersion within the moving object is one-dimensional. During the pulse sequence the relative phase difference between any two points in the object is independent of the object position with respect to the gradient fields. Thus, the phase dispersion is also completely refocused at the center of the echo. The net phase of the total echo signal, however, is shifted in a way dependent on the applied gradient strength, the pulse sequence timing, and the object velocity similar to that in phase-contrast angiography. For very small velocities this phase shift is directly proportional to the object velocity. Thus, the result of coherent translations is a net phase shift without signal losses (Fig 1, *e*). During signal averaging, which is usually necessary with MR spectroscopy to increase the signal-to-noise ratio, such phase shifts, usually incoherent from acquisition

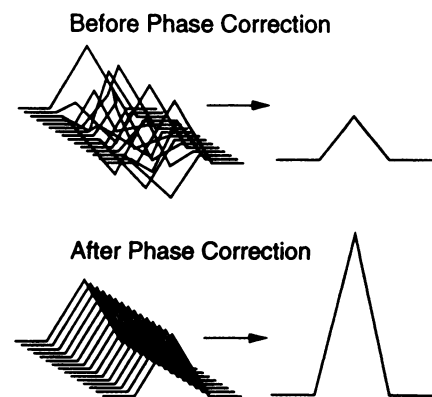


**Figure 2.** Motion artifact compensation in localized spectroscopy. Top: Motion-related phase errors in individual acquisitions, which are usually incoherent, lead to signal loss at averaging. Bottom: Phase correction of individual data traces restores phase coherence and avoids signal loss.

to acquisition, lead to signal losses. Bulk rotations, by contrast, lead to phase errors and signal losses in individual acquisitions, since the gradient directions relative to orientation of the volume of interest change during the pulse sequence, leading to incomplete refocusing of the phase dispersion imposed by the initial gradient pulses. Similarly, more complex forms of macroscopic incoherent motion such as turbulence and shear lead to phase errors and signal losses as well (Fig 1, *f*). In vivo, such macroscopic motion-related signal

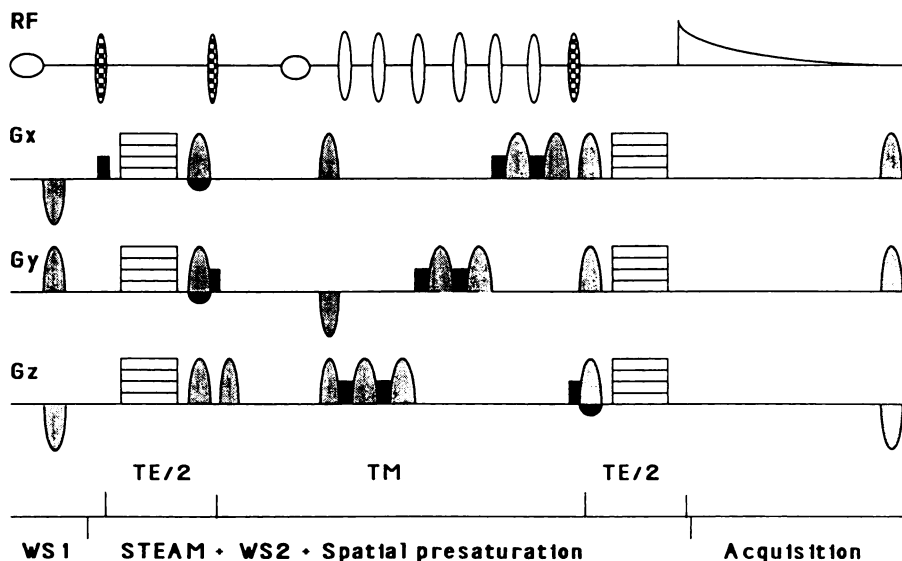


**Figure 3.** Localized proton spectroscopy pulse sequence based on STEAM inner-volume selection and outer-volume suppression during mixing time (TM). Chemical shift-selective (CHES) water suppression pulses are applied before the STEAM localization (WS1) and during TM (WS2) prior to spatial suppression. Suppression radio-frequency pulses are depicted as open symbols. The STEAM radio-frequency pulses are shown as stippled ovals. Section-selection gradients and rephasing gradients are in black, and gradient dephasing pulses are in gray. Data acquisition starts at the top of the echo.

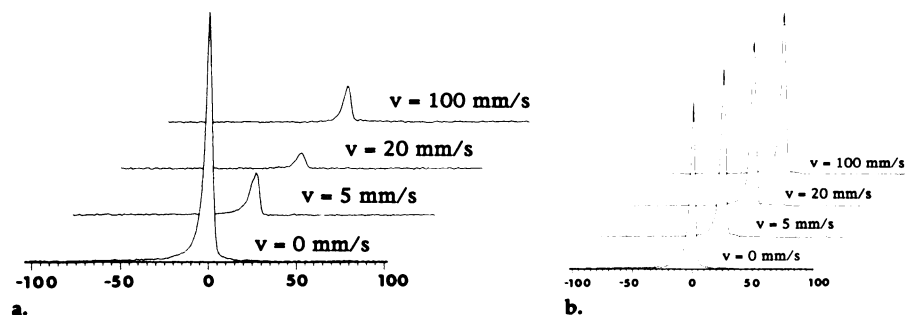


**Figure 4.** Motion compensation in an agarose gel phantom. Phantom motion was oscillatory along the z axis, with a maximal amplitude of 20 mm. Maximal velocity varied from 0 to 100 mm/sec. Localized spectra of unsuppressed water were acquired with maximal-diffusion gradients. Parameters included 3,000/60, a TM of 200 msec, a  $3 \times 3 \times 2$ -cm<sup>3</sup> voxel, and 64 acquisitions. *s* = second, *v* = velocity. (a) Graph shows strong signal losses with conventional averaging due to motion-induced phase errors in individual acquisitions. (b) Graph shows complete signal recovery with phase compensation in individual data traces.

losses are superimposed on diffusion-related signal losses and lead to an overestimation of diffusion coefficients (16).

Linear motion-related phase errors in individual acquisitions and possible signal losses with signal averaging can be corrected, if each acquisition is stored individually and phase corrected prior to signal averaging (Fig 2). Such a phase correction can be performed in the time domain or in the frequency domain, provided the signal-to-noise ratio in individual acquisitions is large enough. In this study we performed the phase correction in the frequency domain to investigate the possibility of using the suppressed water signal, which can be adjusted to be well above the noise level without impairing the detection of metabolite signals, as a tracer signal for the phase correction. The phase relationship between water and metabolite signals was investigated in detail

to validate this approach (see Results). In brain tissue the majority of water arises from intra- and extracellular water, which moves coherently with the cells. Water flowing in blood vessels and perfusing water in capillaries, which may have different motion patterns, constitute only a small fraction of total tissue water (2).

Signal losses due to nontranslational motion are more difficult to compensate. In the brain such motions are primarily due to cardiac-related cerebrospinal fluid pulsations, which give rise to complex motion patterns (17–19), and to involuntary head movements due to breathing and swallowing. Although it is possible to employ gradient compensation to reduce these signal losses, the complexity of in vivo movements requires lengthy, higher-order compensation schemes that severely curtail diffusion sensitivity. Cardiac gating to periods of minimal cerebrospinal fluid

motion can be used to reduce such signal losses. If spectra are acquired under partial saturation conditions, irregularities of heartbeat and respiration can introduce additional signal errors. In general, a compromise between excessive experiment times under fully relaxed conditions and T1-related signal errors due to variations in heartbeat must be sought. It is fortunate that most of these motions contain major linear motion components that can be corrected for by means of the above-described phase correction algorithm.

## Materials

Informed consent was obtained from all volunteers in this study. Ten healthy volunteers (nine male, one female) whose ages ranged from 26 to 31 years were studied.

All measurements were performed with a clinical 1.5-T Signa scanner (GE Medical Systems, Milwaukee, Wis) equipped with actively shielded gradients of 10 mT/m maximum strength. The field inhomogeneity of the magnet over a spherical volume of 20 cm was generally less than 20 Hz (peak to peak). A standard quadrature head coil and a specially designed head holder to reduce involuntary motion were used. Multisection, axial gradient-echo images with 500/5 (repetition time msec/TE msec) and a flip angle of 45° were acquired to locate the volume of interest.

## Methods

A water-suppressed, stimulated-echo acquisition mode (STEAM) pulse sequence (Fig 3) was used for localized diffusion measurements in vivo (20–22). Compared with spin-echo measurements, the method reduces T2 losses at the expense of T1 losses during the mixing period (TM). Such losses are usually less severe in vivo, since in most tissues T1 is much longer than T2. Diffusion gradients are applied during the TE/2 period to dephase moving spins. The TM period can be elongated to provide adequate diffusion sensitivity even at moderate gradient strengths and at relatively short TEs.

We have previously shown that outside signal contaminations, which may degrade localized spectra, can be strongly reduced by combining STEAM inner-volume excitation with complete outer-volume suppression (23). Here we use a similar approach but apply the outer volume suppression during the TM period to minimize the time delay between spatial suppression and signal acquisition, thus reducing effects from differential T1 relaxation. Six section-selective sinc pulses with subsequent gradient dephasing for complete spatial suppression around the volume of interest were applied. Four-side-lobe sinc pulses of 4.5 msec duration in combination with 10-msec gradient dephasing pulses were used. The positions and widths of the spatial suppression sections were computed automatically on the basis of dimensions and position of the volume of interest and predefined outer limits for the

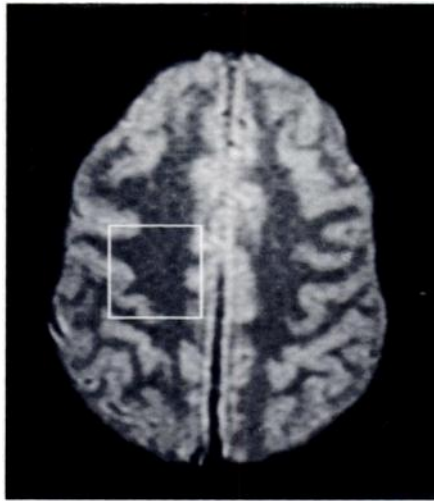


**Figure 5.** Axial GRASS localizer. Spectroscopic volume selection in white matter is indicated by the box. The pulse sequence parameters for this MR image were 600/5, with a flip angle of 45°.

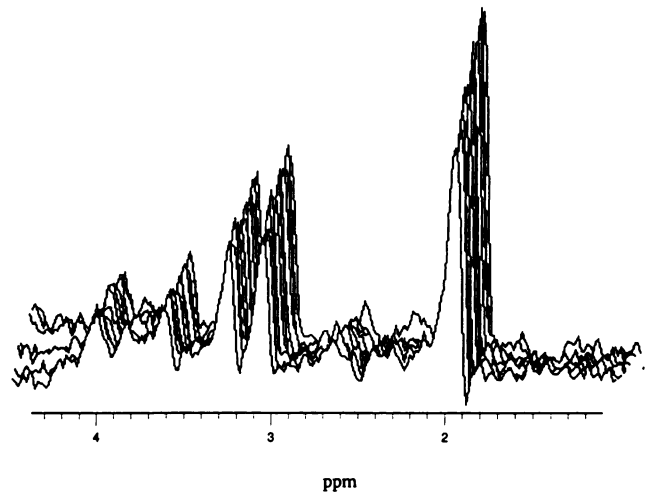


**Figure 6.** Localized proton spectra of human brain tissue acquired with 11 different diffusion gradient strengths. Spectra displaying major resonances from Cho (3.24 ppm), Cr-PCr (3.02 ppm), and NAA (2.01 ppm) are plotted with decreasing diffusion gradient strengths (10–0 mT/m in 1 mT/m steps). Spectral artifacts are negligible even with maximum diffusion gradients applied. Parameters were 3,000/60, a TM of 200 msec,  $3 \times 3 \times 2\text{-cm}^3$  voxel, and 64 acquisitions.

presaturation sections. A gap of 5 mm between the suppression sections and the volume of interest reduced signal losses due to imperfections of the suppression section profiles.

Water suppression was obtained by means of two CHESS pulses (24), one prior to spatial localization and the second during TM. Sinc pulses of 75 Hz bandwidth without side lobes, filtered with a Hanning window, were used. The flip angle of the initial water suppression pulse was larger than 90° due to longitudinal relaxation during the pulse sequence. The duration of the dephasing gradient pulses were 30 msec for the initial CHESS cycle and 10 msec for the CHESS cycle in the TM period.

Two-side-lobe sinc pulses of 1.6 msec duration filtered with a Hanning window were used for the STEAM section selection. The TE and TM dephasing gradient pulses had a duration of 4 and 6 msec, respectively. Diffusion sensitizing gradients of 18-msec duration were simultaneously applied along the x, y, and z axes. Possible residual transverse magnetization after data acquisition was dephased with post-acquisition gradient pulses of 5-msec width. The pulse sequence was tuned for gradient slew rate effects by centering the radio-frequency pulses with respect to the gradient envelope. No phase cycling was used. All dephasing gradient pulses had a strength of 10 mT/m. Gradient ramps were 0.5 msec long.

The gradient switching scheme was optimized to avoid unwanted gradient-recalled echoes by choosing different gradient crusher directions (25) for the spatial suppression and for the STEAM volume selection as shown in Fig 3. To reduce possible artifacts due to residual eddy currents, sinusoidal crusher gradient waveforms and additional gradient delays were employed before the STEAM section-selection

pulses, diffusion gradients, and data acquisition.

Spectroscopic measurements were performed with 3,000/60 and a TM of 200 msec. Spectra were acquired from a  $3 \times 3 \times 2\text{-cm}^3$  voxel in the right hemisphere above the ventricles, containing mostly white matter. Peripheral gating was used to compensate for cardiac-related brain and cerebrospinal fluid pulsations. A time delay of 300 msec between the systolic wave and the beginning of the pulse sequence was found to minimize motion-induced signal amplitude variations (see Results). Manual shimming on the selected voxel was performed with linear gradient shims by maximizing the absorption peak height of the water resonance. We typically obtained absorption line widths of 4–5 Hz (full-width at half-maximum). Water suppression (approximately 200-fold) was adjusted to obtain a residual water signal that dominated the spectrum and served as a tracer signal for signal postprocessing. The residual water signal was undistorted except for a small phase shift with respect to the metabolite resonances that did not vary substantially between acquisitions (see Results).

Spectra were acquired randomly at 11 different diffusion gradient values ranging from 0 to 10 mT/m with 1 mT/m increments. The gradient factor  $b$  determined by means of numeric integration (26) ranged from 59 to 2,200  $\text{sec}/\text{mm}^2$ . All field gradients,  $G(t')$ , applied during the pulse sequence were taken into account. Section selection and TE dephasing gradient pulses contributed greatly to the  $b$  factor, both through cross terms with the diffusion gradients and through quadratic terms. For each diffusion gradient value, 64 acquisitions were individually recorded into a two-dimensional data set. The spectral width was 1 kHz, with a digital resolu-

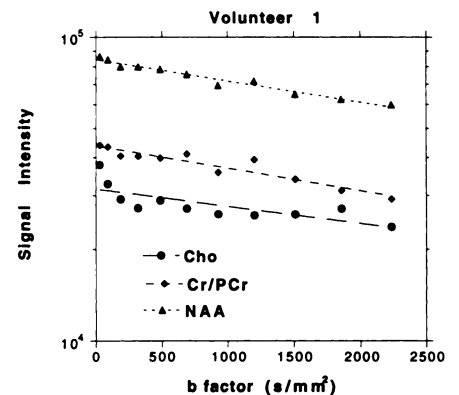


**Figure 7.** Signal intensities for Cho, Cr-PCr, and NAA versus gradient factor  $b$  for data from Figure 6. Dashed curves indicate computed exponential fits to Equation (1).

tion of 1 Hz. Total experiment time was 70 minutes, including imaging, shimming, and water suppression.

Data processing of the two-dimensional data sets was performed with a Sun workstation and SAGE spectral analysis software (GE Medical Systems). It consisted of exponential apodization with 2 Hz, zero filling to 2,048 complex points, Fourier transformation, and automatic zero-order phase correction for each individual signal trace prior to spectral summation. Since the phase of the residual water signal was slightly different from that of the metabolite signals (see Results), summed spectra were manually zero-order phase corrected to optimize the absorption mode signal of the metabolites. After correction for possible residual baseline offsets, peak heights of Cho, Cr-PCr, and NAA were obtained by means of automatic peak picking and fitted to single exponentials by using Equation (1).

## RESULTS

### Method Validation

Volume selection properties of the pulse sequence were investigated in phantoms by imaging the selected voxel with and without outer-volume suppression. The voxel definition was found to be substantially improved with outer-volume suppression. Residual outside signals were reduced by more than 100-fold, while the signal from the selected volume was reduced by less than 5%.

In phantoms, spectral distortion was insignificant and spectral line widths increased by less than 1 Hz when maximal-diffusion gradients were applied. Instrument stability was assessed by observing the non-suppressed water resonance with maximal-diffusion gradients applied. Over periods of 10 minutes the amplitude was stable to within 3% and the phase was stable to within 5°.

Compensation of linear motion effects was verified with an agarose gel phantom that moved along the magnet axis under software control. The motion was oscillatory, with adjustable amplitudes and maximal velocities reaching up to 100 mm/sec. The voxel selection and experimental parameters were the same as for the in vivo studies performed with maximal-diffusion gradients. Figure 4a shows spectra of the unsuppressed water resonance obtained with conventional averaging of 64 acquisitions. Strong signal losses are evident, even at table speeds as low as 5 mm/sec. With phase correction of individual acquisitions the signal is recovered for table velocities of up to 100 mm/sec (Fig 4b).

Diffusion measurements of phantoms with 10 mmol/L solutions of Cho and NAA were conducted to compare the results with in vivo results and to investigate the performance of the localization method (27). The in vitro metabolite diffusion coefficients at 37°C were  $1.3 \times 10^{-3} \text{ mm}^2/\text{sec} \pm 0.03 \times 10^{-3}$  (mean  $\pm$  standard deviation) for Cho and  $0.9 \times 10^{-3} \text{ mm}^2/\text{sec} \pm 0.03 \times 10^{-3}$  for NAA. Water diffusion at 21°C was determined to be  $1.95 \times 10^{-3} \text{ mm}^2/\text{sec} \pm 0.05 \times 10^{-3}$ , which is in reasonable agreement with literature values between  $2.0 \times 10^{-3} \text{ mm}^2/\text{sec}$  (3) and  $2.09 \times 10^{-3} \text{ mm}^2/\text{sec}$  (interpolated from reference 28).

Motion-induced signal errors in vivo were investigated with the non-suppressed water signal acquired under the same conditions as for the metabolite measurements by using maximal diffusion gradients. Both

with and without peripheral gating, the signal phase was extremely unstable and almost random. Without peripheral gating, the signal amplitude in individual acquisitions exhibited strong variations, sometimes with almost complete signal losses. With peripheral gating these signal amplitude variations were strongly reduced. By varying the time delay between the systolic wave and the pulse sequence trigger from 0 to 600 msec, minimal amplitude fluctuations (usually less than 20%) were found at a delay time of approximately 300 msec. Without peripheral gating or phase correction, diffusion coefficients were grossly overestimated.

The phase relationship between the water and metabolite signals was investigated by selecting a larger ( $38 \times 68 \times 20 \text{ mm}$ ) volume, mostly in white matter, to detect metabolite signals with adequate signal-to-noise ratios in individual acquisitions. The average phase difference between water and NAA, as determined with maximal diffusion gradients, was  $25^\circ \pm 24^\circ$ . The residual phase fluctuations (standard deviation,  $24^\circ$ ) corresponded to the noise level.

### In Vivo Diffusion Coefficients

Spectroscopic volume localization was the same for all volunteers (Fig 5). As an example, Figure 6 shows a typical series of spectra acquired with 11 different diffusion gradient amplitudes. Signals from NAA (2.01 ppm, 2.52 ppm), glutamine-glutamate (2.35 ppm, 3.8 ppm), Cr-PCr (3.02 ppm, 3.93 ppm), Cho (2.24 ppm), and inositols (3.54 ppm) are detectable. Spectral overlap from adjacent J-coupled resonances (eg, glutamine-glutamate) at the position of NAA was minimal, as seen in Figure 6, because of the relatively long TE chosen. Owing to signal-to-noise constraints, only singlet resonances from Cho, Cr-PCr, and NAA were quantitated (Fig 7). Best curve-fitting results were usually obtained for NAA, while data scatter for Cr-PCr and Cho was slightly larger. Metabolite diffusion coefficients obtained in 10 healthy volunteers are summarized in the Table. For most subjects, with the exception of subject 7, the apparent diffusion coefficient of NAA was slightly larger than that of Cr-PCr or Cho. The cause for the deviation in subject 7 is not known and may be related to motion. Reproducibility was verified in two volunteers (subjects 9 and 10), giving consistent results within experimental errors.

The apparent diffusion coefficient

of the unsuppressed water resonance ( $0.65 \times 10^{-3} \text{ mm}^2/\text{sec} \pm 0.02 \times 10^{-3}$ ) obtained in separate experiments was similar to previously published results obtained with diffusion-sensitive imaging (3).

## DISCUSSION

Localized diffusion spectroscopy in vivo in the human brain appears to be feasible with adequate spectroscopic localization and motion compensation by means of phase correction of individual acquisitions. While previous measurements in vivo required complete immobilization to avoid motion-induced signal losses, we were able to investigate conscious human subjects.

The spectral quality obtained in human brain tissue, even with the strongest diffusion gradients applied, was similar to that of conventional non-diffusion-weighted spectroscopy, indicating that eddy current-induced line broadening and spectral distortions were negligible despite the use of long gradient pulses. The reproducibility of metabolite measurements was largely dependent on their signal-to-noise ratio, which favors NAA over Cho and Cr-PCr. In addition, Cho and Cr-PCr, which are closer to the water resonance, are more sensitive to small changes in water suppression with head motion and cardiac-related brain pulsations, which might introduce baseline offsets.

At inspection of individual data traces it became evident that signal errors consisted mostly of phase errors rather than amplitude losses, indicating that linear motion patterns (possibly from movements of the whole head) dominated in measurements obtained with peripheral gating. Signal errors due to linear motion, along with small zero-order phase shifts due to residual eddy currents, could be completely removed by means of data postprocessing with zero-order phase correction and did not introduce spectral distortions. As the degree of amplitude errors varied slightly from subject to subject, depending on factors such as breathing and swallowing, it was not possible to completely rule out the influence of nonlinear motion on the measurements. This may be partly responsible for inter- and intraindividual measurement variations. Our own experience with diffusion spectroscopy in anesthetized and paralyzed monkeys (Jordan EK, Posse S, Cuenod CA, Le Bihan D; unpublished data, 1992), which yields only slightly smaller me-

tabolite diffusion coefficients, indicates that such errors in human measurements are probably less than 20%.

Metabolite diffusion coefficients measured in 10 subjects were approximately an order of magnitude smaller than those previously reported in humans (11) and more consistent with measurements in anesthetized and paralyzed animals (9,10). For example, Moonen and co-workers reported NAA diffusion coefficients in cat brain tissue that at a diffusion time of 200 msec ranged from  $0.09 \cdot 10^{-3}$  to  $0.23 \cdot 10^{-3}$  mm<sup>2</sup>/sec, depending on the gradient direction relative to the fiber orientation (interpolated from reference 9). Even at diffusion times as short as 50 msec they found anisotropy indicating bulk effects. By contrast, Merboldt and co-workers recently reported isotropic metabolite diffusion in rat brain tissue at a diffusion time of 25 msec (10). They measured a slightly larger diffusion coefficient for Cho ( $0.3 \cdot 10^{-3}$  mm<sup>2</sup>/sec) than for NAA ( $0.25 \cdot 10^{-3}$  mm<sup>2</sup>/sec).

In humans, apparent metabolite diffusion coefficients were considerably smaller than that of water; this finding may be attributable to differences in molecular weight, to hydration layers around the metabolites, and to hindrance by macromolecular compounds. Apparent metabolite diffusion coefficients measured in vivo were considerably smaller than those measured in vitro, indicating dominating influences of motion restriction by membranes and hindrance due to macromolecular compounds at the long diffusion time used in this study. This finding may also explain why the diffusion coefficients of major metabolites are similar in vivo, in contrast to our in vitro measurements. At shorter diffusion times for which motion restriction is expected to be less severe, more pronounced differences in metabolite diffusion coefficients may be observable, similar to those in rat brain tissue reported by Merboldt and co-workers (10).

When interpreting in vivo results, it becomes evident that motion restriction plays a major role, especially with longer diffusion times, at which apparent diffusion coefficients become anisotropic. In the human study presented here, in which diffusional anisotropy is expected to be similar to that in cat brain tissue (9), the position of the volume of interest and the orientation of diffusion gradients may have influenced the measurement of diffusion coefficients. We are currently investigating metabolite diffu-

**Apparent Metabolite Diffusion Coefficients in Brain White Matter of 10 Healthy Volunteers**

Subject	Cho	Cr-PCr	NAA
1	0.16 (0.03)	0.19 (0.02)	0.22 (0.01)
2	0.10 (0.03)	0.14 (0.03)	0.17 (0.02)
3	0.11 (0.03)	0.17 (0.02)	0.18 (0.01)
4	0.12 (0.03)	0.16 (0.03)	0.19 (0.02)
5	0.11 (0.02)	0.14 (0.02)	0.17 (0.01)
6	0.10 (0.03)	0.10 (0.03)	0.17 (0.02)
7	0.20 (0.03)	0.21 (0.02)	0.20 (0.02)
8	0.10 (0.03)	0.11 (0.02)	0.15 (0.02)
9	0.11 (0.03)	0.12 (0.02)	0.18 (0.01)
9*	0.13 (0.02)	0.15 (0.02)	0.18 (0.01)
10	0.13 (0.03)	0.14 (0.03)	0.16 (0.02)
10*	0.15 (0.03)	0.14 (0.03)	0.16 (0.02)
Mean	0.13 (0.03)	0.15 (0.03)	0.18 (0.02)

Note.—Values are to be multiplied by  $10^{-3}$  to represent square millimeters per second. Values in parentheses are standard deviations.  
\* Measurement repeated in same volunteer.

sion in relation to fiber orientation and voxel position, for NAA in particular, to assess diffusional anisotropy. Experiments with different diffusion times are under development to evaluate restriction effects. While it is feasible to reach short diffusion times in small-bore imagers with strong gradients, measurements with whole-body imagers are limited by the available gradient strengths. Local high-flux gradient coils may help to reach shorter diffusion times in human experiments.

Tissue-related magnetic field gradients, which were not taken into account during calculation of the gradient factor b introduce the possibility of overestimation of diffusion coefficients. While macroscopic field gradients could be compensated by means of localized shimming, the contribution of subvoxel field gradients is unknown and remains to be addressed (29). Proton spectroscopy in the human brain at field strengths of 1–4 T indicates that line widths in brain tissue are dominated by microscopic susceptibility effects rather than by transverse relaxation (30,31). Local differences in susceptibility due to deoxyhemoglobin in small blood vessels, for example, can give rise to substantial local gradients. Our results at 1.5 T, however, are largely consistent with measurements by Moonen and co-workers at 4.7 T (9), with which susceptibility effects are expected to be much stronger. This indicates that local gradients, on average, are small compared with the applied diffusion gradients.

At short echo times, a number of relatively weak resonances with complex J-coupling or short transverse relaxation times are detectable (23,32) and may exhibit interesting diffusion

properties. To assess these resonances at short echo times, it is necessary to use stronger local high-flux gradient coils and more sensitive radio-frequency coils. In cortical regions, for example, surface coils will strongly improve the signal-to-noise ratio. With more complex spectral patterns, however, spectral overlap becomes a problem and reliable data analysis methods must be developed to distinguish small differences in overlapping resonances.

As reported above, signal amplitude variations in individual data traces due to nontranslational motion may lead to an overestimation of diffusion coefficients. To improve the robustness of the method, we are investigating statistical methods to reject individual data traces that exhibit excessive signal losses due to nonlinear motion. We are also investigating the feasibility of diffusion spectroscopic imaging to simultaneously measure diffusion in multiple voxels. As expected, ghosting artifacts due to the strong motion sensitization proved to be a major problem. As a first step, we developed a robust motion artifact compensation method for diffusion-sensitive spectroscopic imaging (33).

The method presented in this article may be valuable for the investigation of metabolite mobility in normal human brain tissue similar to measurements in animal brain. By using NAA as a neuronal marker, it may be possible to investigate cell- and metabolite-specific mechanisms of motion restriction. Applications to disease processes such as white matter diseases, brain atrophy, and acute stroke will be of particular interest. Water diffusion in acute stroke, for example, which is reduced in isch-

emic lesions, is not yet fully understood. Intracellular and tissue-specific markers like Cho, Cr-PCr, NAA, and inositol may provide further information about physiologic changes in ischemic tissue and the underlying mechanisms of altered water diffusion. Finally, diffusion represents a new degree of freedom to characterize *in vivo* proton spectra that at clinical field strengths suffer from densely packed spectral information. If, for example, several compounds with different diffusion properties contribute to a single resonance line, diffusion spectroscopy may help to distinguish them. It is possible, for instance, to suppress rapidly diffusing compounds such as water and certain metabolites while retaining slowly diffusing compounds such as lipids and proteins (34). Diffusion spectroscopy may thus provide new opportunities for tissue characterization and functional studies. ■

**Acknowledgments:** We are indebted to Pierre Germain, BS, for his help with implementing software routines for automated data processing. We gratefully acknowledge Joseph A. Frank, MD, for supporting this work.

#### References

1. Le Bihan D, Breton E, Lallemand D, Grenier P, Canabis EA, Laval-Jeantet M. MR imaging of intravoxel incoherent motion: applications to diffusion and perfusion in neurologic disorders. *Radiology* 1986; 161:401-407.
2. Le Bihan D, Breton E, Lallemand D, Aubin M, Vignaud J, Laval-Jeantet M. Separation of diffusion and perfusion in intravoxel incoherent motion (IVIM) MR imaging. *Radiology* 1988; 168:497-505.
3. Le Bihan D. Molecular diffusion nuclear magnetic resonance imaging. *Magn Reson Q* 1990; 7:1-30.
4. Moseley ME, Cohen Y, Mintorovitch J, et al. Diffusion-weighted MR imaging of water diffusion in cat central nervous system. *Radiology* 1990; 176:439-446.
5. Rutherford MA, Cowan FM, Manzur AY, et al. MR imaging of anisotropically restricted diffusion in the brain of neonates and infants. *J Comput Assist Tomogr* 1991; 15:188-198.
6. Moseley M, Kucharczyk J, Kurhanewicz J, Norman D. Diffusion-weighted MR imaging of acute stroke: correlation with T2-weighted and magnetic susceptibility-enhanced MR imaging in cats. *AJNR* 1990; 11:423-429.
7. Warach S, Chien D, Li W, Ronthal M, Edelman RR. Fast magnetic resonance diffusion-weighted imaging of acute human stroke. *Neurology* 1992; 42:1717-1723.
8. Moonen CTW, van Zijl PCM, Le Bihan D, DesPres D. *In vivo* NMR diffusion spectroscopy: 31P applications to phosphorus metabolites in muscle. *Magn Reson Med* 1990; 13:467-477.
9. Moonen CTW, van Gelderen P, van Zijl PCM, DesPres D, Olson A. The translational mobility of *N*-acetylaspartate in cat brain as measured by localized proton NMR spectroscopy (abstr). In: Book of abstracts: Society of Magnetic Resonance in Medicine 1991. Berkeley, Calif: Society of Magnetic Resonance in Medicine, 1991; 141.
10. Merboldt KD, Höstermann D, Hänicke W, Bruhn H, Frahm J. Molecular self-diffusion of intracellular metabolites in rat brain *in vivo* investigated by localized proton NMR diffusion spectroscopy. *Magn Reson Med* 1993; 29:125-129.
11. Moonen CTW, von Kienlin M, van Zijl PCM, et al. Comparison of single shot localization methods (STEAM and PRESS) for *in vivo* proton NMR spectroscopy. *NMR Biomed* 1989; 2:201-208.
12. Gyngell ML, Frahm J, Merboldt KD, Hänicke W, Bruhn H, Frahm J. Molecular self-diffusion of intracellular metabolites in rat brain *in vivo* investigated by localized proton NMR diffusion spectroscopy. *J Magn Reson* 1988; 77:596-598.
13. Klammer F, Kimmich R. Volume selective and spectroscopically resolved NMR investigation of diffusion and relaxation in fertilized hen eggs. *Phys Med Biol* 1990; 35:67-79.
14. Posse S, Cuenod CA, Jordon EK, Le Bihan D. *In vivo* 1H diffusion spectroscopy in human brain (abstr). In: Book of abstracts: Society of Magnetic Resonance in Medicine 1992. Berkeley, Calif: Society of Magnetic Resonance in Medicine, 1992; 2141.
15. Stejskal EO, Tanner JE. Spin diffusion measurements: spin echoes in the presence of time-dependent field gradients. *J Chem Phys* 1965; 42:288-292.
16. Chenevert T, Brunberg J, Pipe J. Anisotropic diffusion within human white matter: demonstration with NMR techniques *in vivo*. *Radiology* 1991; 177:401-405.
17. Feinberg DA, Mark AS. Human brain motion and cerebrospinal fluid circulation demonstrated with MR velocity imaging. *Radiology* 1987; 163:793-799.
18. Poncet BP, Weeden VJ, Weisskopf RM, Cohen MS. Brain parenchyma motion: measurement with cine echo-planar MR imaging. *Radiology* 1992; 185:645-651.
19. Enzmann DR, Pelc NJ. Brain motion: measurement with phase-contrast MR imaging. *Radiology* 1992; 185:653-660.
20. Granot J. Selected volume excitation using stimulated echoes (VEST): applications to spatially localized spectroscopy and imaging. *J Magn Reson* 1986; 70:488-492.
21. Kimmich R, Hoepfel D. Volume selective multipulse spin echo spectroscopy. *J Magn Reson* 1987; 72:379-384.
22. Frahm J, Merboldt KD, Hänicke W. Localized proton spectroscopy using stimulated echoes. *J Magn Reson* 1987; 72:502-508.
23. Posse S, Schuknecht B, Smith ME, van Zijl PCM, Herschkowitz N, Moonen CTW. Short echo time proton spectroscopic imaging. *J Comput Assist Tomogr* 1993; 17:1-14.
24. Haase A, Frahm J, Hänicke W, Matthaei D. 1H NMR chemical shift selective (CHESS) imaging. *Phys Med Biol* 1985; 30:341-344.
25. Moonen CTW, van Zijl PCM. Highly effective water suppression for *in vivo* proton NMR spectroscopy (DRYSTEAM). *J Magn Reson* 1990; 88:28-41.
26. Le Bihan D, Cuenod CA, Posse S. Determination of the gradient factor *b* in localized diffusion 1H spectroscopy (abstr). In: Book of abstracts: Society of Magnetic Resonance in Medicine 1992. Berkeley, Calif: Society of Magnetic Resonance in Medicine, 1992; 1218.
27. Cuenod CA, Posse S, Le Bihan D. Relationship between diffusion and temperature for *N*-acetyl aspartate and choline: a localized 1H NMR spectroscopy study (abstr). In: Book of abstracts: Society of Magnetic Resonance in Medicine. Berkeley, Calif: Society of Magnetic Resonance in Medicine, 1992; 1215.
28. Mills R. Self diffusion in normal and heavy water in the range 1-45°. *J Chem Phys* 1973; 77:685-688.
29. Zhong J, Kennan RP, Gore JC. Effects of susceptibility variations on NMR measurements of diffusion. *J Magn Reson* 1991; 95:267-280.
30. Sauter R, Loeffler W, Bruhn H, Frahm J. The human brain: localized H-1 MR spectroscopy at 1.0 T. *Radiology* 1990; 176:221-224.
31. Barfuss H, Fischer H, Hentschel D, et al. *In vivo* magnetic resonance imaging and spectroscopy of humans with a 4 Tesla whole-body magnet. *NMR Biomed* 1990; 3:31-45.
32. Frahm J, Bruhn H, Gyngell ML, Merboldt KD, Hänicke W, Sauter R. Localized proton NMR spectroscopy in different regions of the human brain *in vivo*: relaxation times and concentrations of cerebral metabolites. *Magn Reson Med* 1989; 11:47-63.
33. Posse S, Cuenod CA, Le Bihan D. Motion artifact compensation in 1H spectroscopic imaging by signal tracking. *J Magn Reson* (in press).
34. Van Zijl PCM, Moonen CTW, Faustino P, Peckar J, Kaplan Ofer, Cohan J. Complete separation of intracellular and extracellular information in NMR spectra of perfused cells by diffusion-weighted spectroscopy. *Proc Natl Acad Sci USA* 1991; 88:3228-3232.